

## Variable Hard X-ray Emission From the Central Star of the Eskimo Nebula

MARTÍN A. GUERRERO,<sup>1</sup> JESÚS A. TOALÁ,<sup>2</sup> AND YOU-HUA CHU<sup>3</sup>

<sup>1</sup>*Instituto de Astrofísica de Andalucía, IAA-CSIC, Glorieta de la Astronomía s/n, 18008 Granada, Spain*

<sup>2</sup>*Instituto de Radioastronomía y Astrofísica (IRyA), UNAM Campus Morelia, Apartado postal 3-72, 58090 Morelia, Michoacan, Mexico*

<sup>3</sup>*Institute of Astronomy and Astrophysics, Academia Sinica (ASIAA), Taipei 10617, Taiwan, Republic of China*

(Received January 1, 2018; Revised January 7, 2018; Accepted September 9, 2019)

Submitted to ApJ

### ABSTRACT

The central star of NGC 2392 shows the hardest X-ray emission among central stars of planetary nebulae (CSPNe). The recent discovery of a spectroscopic companion with an orbital period of 1.9 days could provide an explanation for its hard X-ray emission, as well as for the collimation of its fast outflow. Here we analyse the available *Chandra* and *XMM-Newton* X-ray observations to determine accurately the spectral and temporal variation properties of the CSPN of NGC 2392. The X-ray emission can be described by an absorbed thermal plasma model with temperature  $26^{+8}_{-5}$  MK and X-ray luminosity  $(8.7 \pm 1.0) \times 10^{30}$  erg s<sup>-1</sup>. No long-term variability is detected in the X-ray emission level, but the *Chandra* light curve is suggestive of short-term variations with a period  $\sim 0.26$  days. The possible origins of this X-ray emission are discussed. X-ray emission from the coronal activity of a companion or shocks in the stellar wind can be ruled out. Accretion of material from an unseen main-sequence companion onto the CSPN or from the CSPN wind onto a white dwarf companion are the most plausible origins for its hard X-ray emission, although the mismatch between the rotational period of the CSPN and the modulation time-scale of the X-ray emission seems to preclude the former possibility.

*Keywords:* ISM: planetary nebulae: general – ISM: planetary nebulae: individual: NGC 2392 – stars: winds, outflows – (stars:) white dwarfs – X-rays: stars – X-rays: individual (NGC 2392)

### 1. INTRODUCTION

The planetary nebula (PN) NGC 2392, the Eskimo Nebula, shows a double shell morphology with an inner elliptical shell displaying an ensemble of filaments and a round outer shell where a series of wisps resembling the fur on a hood can be seen (O’Dell et al. 2002). This morphology is somewhat peculiar among PNe, but it is not completely unseen (e.g., NGC 7662, Guerrero et al. 2004). Actually, its three-dimensional structure might be similar to those of NGC 6543 and NGC 7009, but at a different viewing angle (García-Díaz et al. 2012).

Everything else in NGC 2392 is atypical. The expansion velocity of its inner shell,  $\sim 120$  km s<sup>-1</sup>, is spectacularly large among elliptical shells of PNe

(Reay et al. 1983; O’Dell & Ball 1985; O’Dell et al. 1990; García-Díaz et al. 2012). Its fast  $\sim 180$  km s<sup>-1</sup> collimated outflow, the first ever detected among PNe (Gieseking et al. 1985), can be traced down to its central star (CSPN), a situation uncommon among collimated outflows of PNe. Its central star exhibits the hardest X-ray emission among CSPNe (Ruiz et al. 2013; Montez et al. 2015). The nebular excitation implied by the bright He II emission relative to H $\beta$  (Danekkar et al. 2012), the He II Zanstra temperature of  $\sim 70,000$  K and even higher energy-balance temperature (Méndez et al. 1992) are too high for the CSPN’s effective temperature of 40,000-45,000 K (Pauldrach et al. 2004; Herald & Bianchi 2011). Furthermore, the difference between the electron temperatures derived from [O III] and [N II] lines is much larger than usual (Barker 1991).

All these unusual properties are suggestive of the presence of an additional source of He ionizing photons and

mechanical momentum within the inner nebular shell of NGC 2392. The fast outflow and the hard X-ray emission from the CSPN, in conjunction with the diffuse soft X-ray emission from hot plasma confined within the inner shell (Guerrero et al. 2005; Ruiz et al. 2013), have been suggested to provide these additional sources of momentum and ionizing photons (Ercolano 2009). Alternatively, a hot ( $\approx 250,000$  K), high-gravity white dwarf (WD) binary companion has been proposed for NGC 2392 (Danekhar et al. 2012), and the recent detection of a spectroscopic binary with an orbital period of 1.9 days support this suggestion (Miszalski et al. 2019). The presence of a binary system at the CSPN of NGC 2392 may finally explain the origin of its hard X-ray emission from the accretion of the wind of the CSPN onto the WD companion (Miszalski et al. 2019), and can also be linked to the currently active collimation and launch of the fast bipolar outflow, which might reveal itself through its fast polar wind (Prinja, & Urbaneja 2014).

To investigate the link between accretion and the hard X-ray emission from the CSPN of NGC 2392, we present in this paper a spectral and temporal variation analysis of pointed *Chandra* and *XMM-Newton* observations. These observations are supplemented with multi-wavelength IR, optical, and UV observations and/or archival data to build a spectral energy distribution (SED) of the CSPN of NGC 2392.

## 2. OBSERVATIONS AND DATA

### 2.1. X-ray Observations

The *XMM-Newton* Observatory observed NGC 2392 in Revolution 790 on 2004 April 2 (Obs.ID.: 0200240301; PI: Y.-H. Chu) using the European Photon Imaging Cameras (EPIC). The two EPIC-MOS cameras were operated in the Full Frame mode, while the EPIC-pn camera was operated in the Extended Full Frame mode. The total observing time was 17.7 ks for both MOS and 14.3 ks for pn. All observations were obtained with the medium optical blocking filter. The *XMM-Newton* pipeline products were processed using the *XMM-Newton* Science Analysis Software (SAS) and the calibration files from the Calibration Access Layer available on 2019 July 1. The event files were screened to eliminate events due to charged particles or associated with periods of high background. For the EPIC-MOS observations, only events with CCD patterns 012 were selected, whereas for the EPIC-pn observation only single pixel events were selected. Time intervals with high background count rates in the background-dominated 10–12 keV energy range (i.e.,  $\geq 0.2$  counts  $\text{s}^{-1}$  for MOS and  $\geq 0.45$  counts  $\text{s}^{-1}$  for pn) were discarded. The re-

sulting exposure times are 17.3 ks, 17.5 ks, and 8.3 ks for MOS1, MOS2, and pn, respectively.

The *Chandra* X-ray Observatory observed NGC 2392 for 57.4 ks on 2007 September 13 (Obs.ID: 7421; PI: M.A. Guerrero). The array for spectroscopy of the Advanced CCD Imaging Spectrometer (ACIS-S) was used and the PN was imaged on the back-illuminated CCD S3 using the VFAINT mode. The data were processed and analysed using the *Chandra* Interactive Analysis of Observations (CIAO) software package (version 4.11; Fruscione et al. 2006). The observations were not affected by high-background events, but periods of time with background count rates above  $0.44$  counts  $\text{s}^{-1}$  or anomalously low at the beginning or end of the observation were excised to allow a fair investigation of the temporal variation of NGC 2392. The final exposure time after this procedure was 50.4 ks.

### 2.2. Complementary Observations and Archival Data

#### 2.2.1. IR Observations

Near-IR *JHK* images and long-slit spectra were obtained with the Near Infrared Camera Spectrometer (NICS) on the 3.5 m Telescopio Nazionale Galileo (TNG) at the Observatorio de El Roque de los Muchachos (ORM) on the island of La Palma, Spain. The detector was a HgCdTe Hawaii 1024 $\times$ 1024 array. The large field camera was used for the imaging observations, yielding a pixel size of  $0''.25$  and a field-of-view of  $4'.2 \times 4'.2$ . The medium-resolution *J*, *H*, and *KB* prisms were used in conjunction with a  $0''.75$  slitwidth for the spectroscopic observations, resulting in a spectral resolution of  $\sim 1,200$ .

We have also used archival mid-IR *Spitzer Space Telescope* Infrared Array Camera (IRAC; Fazio et al. 2004) and Infrared Spectrograph (IRS; Houck et al. 2004) observations of NGC 2392. The *Spitzer* IRAC observations (Prog. ID 30285, PI G. Fazio) consisted of images in the 3.6, 4.5, 5.8, and  $8.0 \mu\text{m}$  bands. The *Spitzer* IRS observations (Prog. ID 30482, PI J.R. Houck) were obtained in Spectral Mapping mode to provide multiple spectra from a 2-D region encompassing the inner shell and the surrounding outer shell of NGC 2392. A spectrum of the CSPN was extracted in the wavelength range from  $5.3$  to  $14.7 \mu\text{m}$ .

#### 2.2.2. Optical and UV Observations

*U*, *B*, and *R* magnitudes of the CSPN of NGC 2392 were adopted from SIMBAD, and *V* and *I* magnitudes from Ciardullo et al. (1999). The *Far-Ultraviolet Spectroscopic Explorer* (*FUSE*) dataset B0320601 and the *International Ultraviolet Explorer* (*IUE*) datasets SWP05230LL and LWR04209LL have been used, pro-

viding sensitive observations in the spectral ranges 905–1185 Å and 1150–3350 Å, respectively.

### 3. HARD X-RAYS OF NGC 2392 CSPN

The *Chandra* observations of NGC 2392 detect a point-like X-ray source at its CSPN, as well as diffuse X-ray emission within the inner nebular shell (Ruiz et al. 2013; Montez et al. 2015). The source at the CSPN of NGC 2392 has a full width at half maximum (FWHM) of  $0''.44 \pm 0''.06$  comparable to that of the point spread function (PSF) of *Chandra* at the ACIS-S aimpoint. Thus, its point-source nature is confirmed. The positional coincidence between the X-ray point-source and the CSPN of NGC 2392 merits careful investigation. The *Chandra* ACIS-S S3 field of view includes 5 point sources with stellar counterparts whose coordinates are available in the USNO 2.0 Catalog. Using the coordinates of these 5 stars, the X-ray and optical positions were registered within  $0''.4$ . The positions of the X-ray point-source detected by *Chandra* near the center of NGC 2392 and the CSPN are coincident within  $0''.2$ . Clearly, the X-ray point source is not associated with the visual companion at  $2''.65$  S-SW of the CSPN (Ciardullo et al. 1999). It is also very unlikely that a foreground star or a background extragalactic source is located exactly along the line of sight toward the CSPN and is responsible for the X-ray point source. It can thus be confidently concluded that the X-ray emission from this point source originates from the CSPN of NGC 2392 or from a source in its close vicinity.

To study the spectral properties and possible variations of the X-ray emission from the CSPN of NGC 2392, we have defined a source region of radius  $1''.5$  centered at its location and a surrounding  $12''.8 \times 16''.0$  elliptical background region representative of the diffuse emission. The point-source at the CSPN of NGC 2392 has a background-subtracted count rate of  $3.3 \pm 0.3$  ACIS-S S3 counts  $\text{ks}^{-1}$  for a total of  $185 \pm 15$  counts. Its X-ray spectrum, shown in black in the left panel of Figure 1, peaks at 0.8–1.0 keV and shows a hard-energy tail that declines steadily to 3 keV, with some residual emission at energies as high as to 4.0 keV. This X-ray spectrum is much harder than that of the diffuse emission (shown in red in the left panel of Fig. 1-left, Guerrero et al. 2005), which peaks at 0.5–0.6 keV and diminishes at energies above 1 keV. Assuming a uniform surface brightness for the diffuse emission, the total diffuse emission within the aperture of the CSPN is  $\leq 12\%$  as high as the background-subtracted point source emission. We have tested different background regions representative of the diffuse emission and found that the X-ray spectrum of the CSPN is unaffected at energies  $\geq 1.0$  keV,

but the contamination of diffuse emission may produce variations up to  $\simeq 10\%$  at energies between 0.6 and 0.9 keV, and up to  $\simeq 40\%$  at energies below 0.5 keV. These results are similar to those presented by Montez et al. (2015).

The likely presence of emission lines between 0.8 and 1.0 keV in the spectrum of the CSPN suggests that it can be interpreted as emission produced by an optically thin plasma. Despite the small number of counts, we have used XSPEC (Arnaud 1996) to obtain a rough fit of this spectrum using an absorbed APEC thin plasma emission model<sup>1</sup> assumed to have the subsolar  $\lesssim 0.25 Z_{\odot}$  stellar abundances derived by Herald & Bianchi (2011) and an absorption column density  $N_{\text{H}}$  of  $9 \times 10^{20} \text{ cm}^{-2}$  corresponding to its optical extinction,  $c_{\text{H}\beta} = 0.225$  (Pottasch et al. 2008). The best-fit model ( $\chi^2/\text{DoF} = 10.6/9 = 1.2$ ) with a temperature  $kT = 2.2_{-0.4}^{+0.7}$  keV is overplotted on the background-subtracted X-ray spectrum in Figure 1-left. This temperature is lower than but consistent with that of  $3.1_{-0.7}^{+1.7}$  keV derived by Montez et al. (2015) assuming solar abundances. If a solar abundance were assumed instead, the temperature of the best fit would rise up to  $5.4 \pm 2.3$  keV, but the quality of the fit would worsen ( $\chi^2/\text{DoF} \simeq 1.6$ ). The absorbed X-ray flux in the 0.3–3.0 keV band is  $1.3 \times 10^{-14} \text{ erg cm}^{-2} \text{ s}^{-1}$ . The *Hipparcos* distance to NGC 2392 of 1150 pc (Perryman et al. 1997) is consistent with the expansion distance of 1300 pc derived by García-Díaz et al. (2015), but the most recent *Gaia* determination implies a larger distance of  $2000 \pm 200$  pc (Kimeswenger & Barría 2018). Using the latter, we derive an intrinsic luminosity in the 0.3–3.0 energy band of  $(8.7 \pm 1.0) \times 10^{30} \text{ erg s}^{-1}$ .

The diffuse X-ray emission of NGC 2392 is spatially unresolved from that of its CSPN in the *XMM-Newton* EPIC observations (Guerrero et al. 2005), but its spectral shape is well described by the *Chandra* ACIS-S S3 spectrum. This can be fitted ( $\chi^2/\text{DoF} = 24.8/21 = 1.2$ ) using an optically thin plasma APEC emission model with nebular abundances and absorption column density (Pottasch et al. 2008) for a temperature  $kT = 0.16_{-0.009}^{+0.015}$  keV (Fig. 1-left). The X-ray luminosity of this diffuse emission is  $(7.2 \pm 0.6) \times 10^{31} \text{ erg s}^{-1}$ . This model for diffuse emission is adopted for the *XMM-Newton* EPIC-pn spectrum (red color in Figure 1-right) to obtain a net hard X-ray excess that can be attributed to the emission from the CSPN. This component has been fit with

<sup>1</sup> We note here that the spectrum of the CSPN of NGC 2392 can also be fitted by a highly absorbed power law, but this seems inconsistent with the low hydrogen column density derived from optical and UV observations.

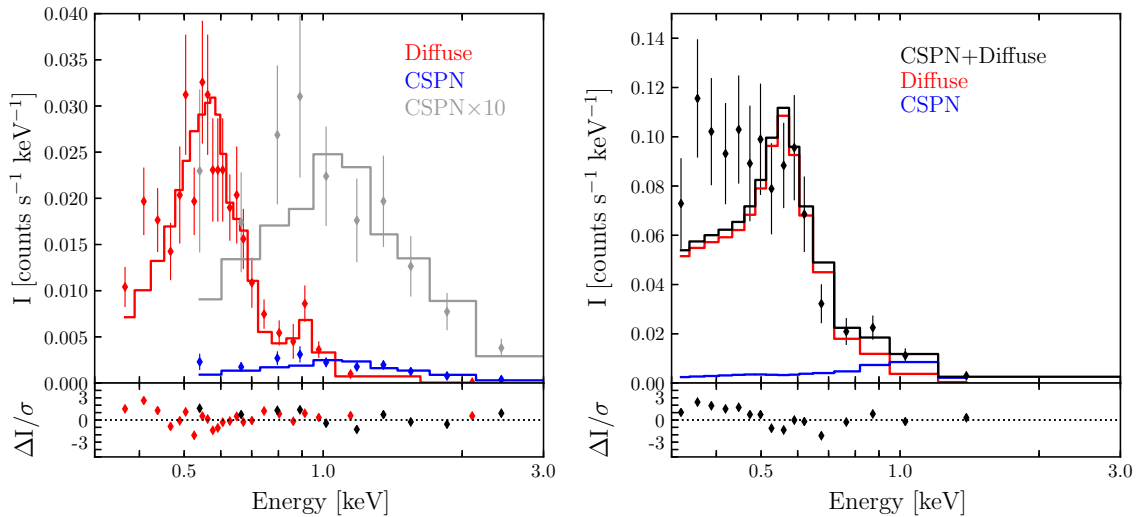


**Figure 1.** *Chandra* ACIS-S S3 (left) and *XMM-Newton* EPIC-pn (right) background-subtracted spectra (dots) of the CSPN of NGC 2392 and its diffuse X-ray emission. The X-ray spectra are overplotted with the best-fit models (solid histograms). The ACIS-S3 spectrum of the CSPN of NGC 2392 and its best-fit model are shown at two different scales to display more clearly its spectral shape and the relative intensities of the CSPN and diffuse emissions. Residuals of the fits are plotted in the lower panels. Both the *Chandra* ACIS-S3 and *XMM-Newton* EPIC-pn spectra of the diffuse emission show residuals in the 0.3–0.45 KeV energy range, which might be attributed to emission from the C VI 0.37 keV and N VI 0.43 keV lines, thus implying higher carbon and nitrogen abundances than those of the stellar wind considered here.

a similar APEC model to that used for the *Chandra* ACIS-S S3 spectrum of the CSPN of NGC 2392. The best-fit model ( $\chi^2/\text{DoF}=33.4/24=1.4$ ) with a temperature  $kT=1.2^{+3.3}_{-0.3}$  keV is overplotted on the background-subtracted X-ray spectrum in Figure 1-right (blue histogram). The absorbed X-ray flux in the 0.3–3.0 keV band is  $8.5 \times 10^{-15}$  erg cm $^{-2}$  s $^{-1}$  and the intrinsic luminosity is  $(7 \pm 3) \times 10^{30}$  erg s $^{-1}$ , which is consistent with that derived from *Chandra*.

The ACIS-S S3 light curve of the CSPN of NGC 2392 in the X-ray energy range 1.0–3.0 keV free from diffuse emission is shown in Figure 2. This X-ray light curve shows some oscillations, very different from the behavior of the light curve of the nebular emission, which is expected to be constant and indeed shows little variations around the mean value all through the duration of the observation. To test for variability, we performed a Kolmogorov-Smirnov test to assess whether these light curves can be ascribed to a Poisson distribution of the photon arrival times. There is a 97% probability that the time arrival of the diffuse X-ray emission follows a Poisson distribution, but only 50% for the CSPN. This same test was applied to three point-sources (2CXO J072908.2+205609, 2CXO J072912.1+210113, and 2CXO J072918.8+205551) in the field of view of ACIS-S S3 with similar count rates to those of the CSPN of NGC 2392, resulting always in probabilities for Poisson distributions of the photon arrival times

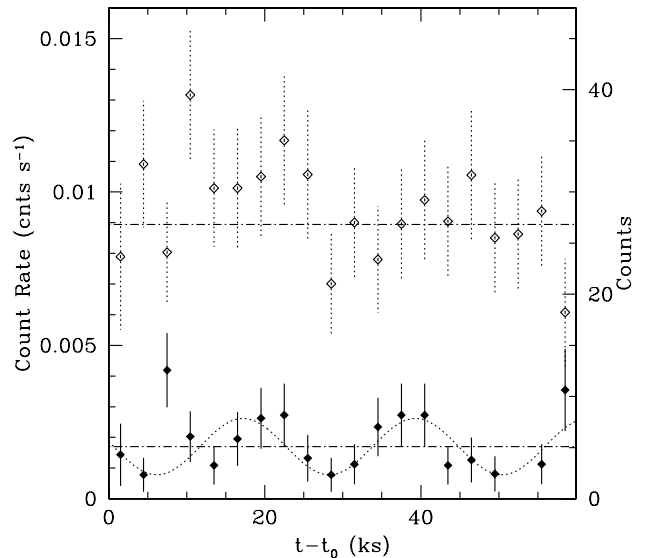


**Figure 2.** *Chandra* ACIS-S S3 light curve of the CSPN of NGC 2392 (solid diamonds) in the energy range 1.0–3.0 keV. The light curve of the diffuse nebular emission in the 0.3–2.0 keV band, which is expected to be constant, is also shown for comparison (open diamonds). The dash-dotted horizontal lines in the light curves mark the averaged count rates. The dotted line corresponds to the best-fit sinusoidal model.

$\gtrsim 85\%$ . Therefore, the X-ray variability of the hard X-ray source at the CSPN of NGC 2392, although not firm, is suggested by the shape of its light curve. A  $\chi^2$

fit of a sinusoidal curve to this light curve (Fig. 2) is indicative of a period  $\simeq 22$  ks ( $\simeq 0.26$  days). This fit has a reduced  $\chi^2$  value of 1.1. For comparison, a similar fit to a constant value has a reduced  $\chi^2$  value of 1.5. This period is consistent with the period  $\simeq 0.253$  days derived from the periodogram obtained using the Lomb-Scargle method, although we reckon that the false alarm probability of 15% which is derived constitutes only a weak indication of periodicity.

#### 4. DISCUSSION

Three possible origins exist for the X-ray emission from the CSPN of NGC 2392 (see, for instance, Montez et al. 2015). They are discussed below.

##### 4.1. Coronal Activity from a Companion

The X-ray emission from the CSPN of NGC 2392 may originate from the coronal activity of an unresolved late-type companion (Guerrero et al. 2001; Montez et al. 2010) whose rotation (and hence its magnetic activity) may have been boosted by the transfer of orbital angular momentum (Soker & Kastner 2002). For late-type dwarf stars of spectral types K and M, the value of  $\log(L_X/L_{\text{bol}})$  is typically  $-5.21$ , although it can increase up to  $-3.56$  for saturated activity (Fleming et al. 1995). Main-sequence stars of earlier spectral types, from A0 to K5, show similar typical and saturated values for  $\log(L_X/L_{\text{bol}})$  (Hünsch, Schmitt, & Voges 1998a; Güdel 2004). As for giant and sub-giant stars, the relationship between spectral type and coronal activity is more complex than for their main sequence counterparts (see the review by Güdel 2004). Giant and sub-giant stars of spectral types later than K1 and earlier than G5 are usually weak X-ray emitters (e.g., Ayres et al. 1981; Haisch et al. 1990; Maggio et al. 1990), with the brightest X-ray sources among G and K stars at  $L_X \leq 10^{31}$  erg s $^{-1}$  and  $\log(L_X/L_{\text{bol}}) < -3$  (Gondoin 2000), although some rapidly rotating G giants with permanent flaring activity can reach X-ray luminosities up to several times  $10^{31}$  erg s $^{-1}$  (Gondoin 2005b, and references therein). A comparison of the plasma temperatures and levels of X-ray emission from the CSPN of NGC 2392 and late type stars is presented in Figure 3. The plasma temperature of the CSPN of NGC 2392 is marginally consistent with those of the coronae of giant late type stars (Hünsch et al. 1999), but its X-ray luminosity is significantly higher. We note that rapidly rotating G giants present similar levels of X-ray emission and, for the case of FK Com, even higher plasma temperatures for the component associated with flares (Gondoin et al. 2002), but the modulation observed in the X-ray light

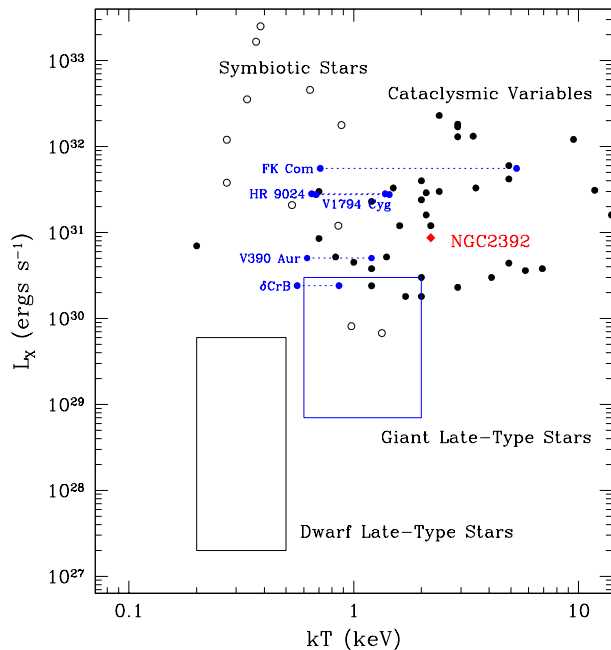


**Figure 3.** Comparison of the location on the  $L_X$  vs.  $kT$  plane of the CSPN of NGC 2392 with these of active stars, cataclysmic variables, and symbiotic stars. The averaged location of dwarf and giant late-type stars (Maggio et al. 1990; Hünsch, Schmitt, & Voges 1998a,b) are marked by black and blue boxes, respectively. Individual rapidly rotating G giant stars with accurate determinations of their X-ray luminosities using two-temperature thermal plasma emission models are marked by solid blue dots at the temperature of each thermal component connected by dotted lines (Gondoin et al. 2002; Gondoin 2003a,b, 2004, 2005a). Individual cataclysmic variables (Eracleous et al. 1991) and symbiotic stars (Mürset et al. 1997; Stute & Sahai 2009; Eze et al. 2010) are marked by filled and open dots, respectively.

curve of NGC 2392 is too fast to be associated with the rotational period of a late-type companion.

##### 4.2. Stellar Wind

A fast stellar wind can generate shocks capable of producing X-ray emission. The shock-in-wind origin for the hard X-ray emission of the CSPN of NGC 2392 is strengthened by the notable variability of its stellar wind (Prinja, & Urbaneja 2014), the intriguing presence of the O VI UV resonance doublet (Herald & Bianchi 2011; Guerrero & De Marco 2013), and an X-ray to bolometric luminosity  $\log(L_X/L_{\text{bol}}) = -6.4$  (for an  $L_{\text{bol}}$  of  $6025 L_{\odot}$ , Pauldrach et al. 2004; Herald & Bianchi 2011) consistent with the value of  $-6.6$  observed in shocks in winds of O stars (Nebot Gómez-Morán & Oskinova 2018). However, the efficiency of conversion of the wind mechanical energy into X-rays for OB stars, in the narrow range  $-3.1 < \log(L_X)/L_w < -2.5$

(Sana et al. 2006), is clearly violated in NGC 2392, with a  $\log(L_X)/L_w = -1.8$ , for a wind luminosity of  $5.4 \times 10^{32}$  erg s $^{-1}$  adopting a terminal wind velocity of 300 km s $^{-1}$  and a mass-loss rate of  $1.9 \times 10^{-8} M_\odot$  yr $^{-1}$  (Herald & Bianchi 2011). More importantly, its stellar wind terminal velocity simply cannot produce hot plasma at a temperature  $kT \sim 2.2$  keV.

In an OB or WR binary system, colliding stellar winds can produce shock-heated plasma at  $10^7$  K ( $kT \sim 1$  keV). The X-ray emission from these systems is characterized by large hydrogen absorption column densities and variability on time-scales of orbital period caused by the varying amount of un-shocked attenuating material along the line of sight. However, none of these fit the observed X-ray emission from the CSPN of NGC 2392.

On a smaller scale, colliding winds are also typical sources of hard X-ray emission in symbiotic stars (SS), interacting binary systems formed by a red giant and a hot (degenerate) companion. The shape of the X-ray spectra of the so-called class  $\beta$  SS is particularly similar to that of the CSPN of NGC 2392; however, their X-ray luminosities are higher because the large mass-loss rate of the red giant star in these systems (Mürset et al. 1997). Only the “low X-ray luminosity SS” such as EG And, SS73 17, and MWC 560 show similar emission levels to those of the CSPN of NGC 2392, but the temperature of the X-ray emitting plasma in these systems is notably lower.

#### 4.3. Accretion

Accretion onto the CSPN or an accretion disk from an unseen companion can also result in hard X-ray emission (Soker & Livio 1994; Mastrodemos & Morris 1998; Reyes-Ruiz & López 1999), e.g., as in quiescent novae and cataclysmic variables (CVs), where strong UV and X-ray emission is typically detected. Such companion would be a main-sequence star of spectral type F0 V or later, as a star with earlier spectral type, such as the B8 V star, whose emission is represented in Figure 4 assuming a black-body model at their temperature and luminosity, would be detectable in the near- and mid-IR SED of the CSPN of NGC 2392. As shown in this figure, a giant star would also be detected at long wavelengths. Quiescent novae have higher X-ray luminosities, typically  $\gtrsim 10^{32}$  erg s $^{-1}$ , and X-ray spectra harder than that of the CSPN of NGC 2392 (Orio et al. 2001), but CVs have similar X-ray luminosities and plasma temperatures as shown in Figure 3. Quiescent novae and CVs, however, are known to exhibit large variability in the optical and X-rays, which do not match those of the CSPN of NGC 2392. Therefore, accretion processes at rates larger than  $10^{-12} M_\odot$  yr $^{-1}$ , typical of

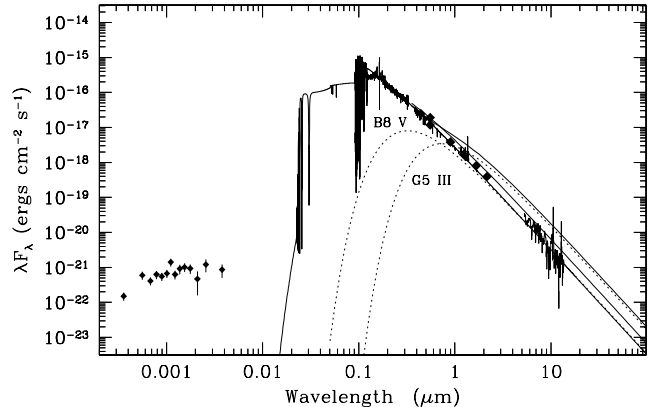


**Figure 4.** X-ray to IR spectral energy distribution (SED) of the CSPN of NGC 2392. The data points and/or spectra have been corrected for extinction to derive the intrinsic SEDs using Cardelli et al. (1989)’s extinction law in the IR, optical, and UV. The emission expected from the star is represented by a NLTE model computed using WMAP, the Tübingen NLTE Model-Atmosphere Package Web interface, at <http://astro.uni-tuebingen.de/~rauch> (Rauch 1997) at a temperature of 45,000 K, a stellar radius of  $0.7 R_\odot$ , and a distance of 2,000 pc assuming a surface He:H ratio of 0.1 by number (thin solid line). The contribution from a B8 V or a G5 III companion (dotted lines) would be detectable in the near- and mid-IR SED of the CSPN of NGC 2392, as shown by the addition of the two spectral components as a thick solid line.

quiescent novae or CVs, can be ruled out as the origin of the hard X-ray emission in the CSPN of NGC 2392. The modulation of  $\sim 0.26$  days in the X-ray light curve of NGC 2392 is twice its rotational period of 0.123 days (Prinja, & Urbaneja 2014), suggesting the X-ray emission does not arise from a hot spot on the surface of the CSPN.

The recent discovery of a binary companion of the CSPN of NGC 2392 provides the tantalizing opportunity to explain the origin of its hard X-ray emission from the accretion of the stellar wind of the CSPN of NGC 2392 onto a relatively massive ( $M \gtrsim 0.6 M_\odot$ ) WD companion or an accretion disk around it (Miszalski et al. 2019). Whereas an accretion disk around this putative WD companion would not produce X-ray emission, for its maximum temperature  $\leq 100,000$  K (Guerrero et al. 2001), accretion directly onto the WD can raise temperatures well up to  $kT \sim 7.6$  keV, well above the observed X-ray temperature of 2.2 keV. The observed X-ray luminosity demands that only  $\sim 1\%$  of the stellar wind from the CSPN of NGC 2392 ( $\dot{M} = 1.9 \times 10^{-8} M_\odot$ , Pauldrach et al. 2004) is actually accreted by the WD companion. In such a case, the modulation observed in the X-ray light curve could be associated with a hot spot onto the surface of the WD and the period would corre-

spond to its rotational period. This scenario, however, is unable to provide an explanation for the presence of the O VI  $\lambda\lambda 1037, 1037$  P-Cygni profiles in the spectrum of the CSPN, which still demands the production of X-rays in its stellar wind (Herald & Bianchi 2011).

The accretion of stellar wind from the CSPN onto the WD can certainly be claimed responsible for the collimation and launch of the fast collimated outflows of NGC 2392. However, we consider it very unlikely that these outflows are the source of the diffuse X-ray emission confined within the inner shell of NGC 2392. First, the outflow speed of  $180 \text{ km s}^{-1}$  is not able to shock-heat material up to X-ray-emitting temperatures. Second, the spatial distributions of the diffuse X-ray emission and collimated outflows do not match; the collimated outflows extends further out from the inner shell (García-Díaz et al. 2012), whereas the diffuse emission is well confined within the inner shell and it does not show any “hot spot” indicative of interactions between the collimated outflow and the nebular material (Ruiz et al. 2013). According to recent hot bubble hydrodynamical simulations (Toalá & Arthur 2016), the stellar wind of the CSPN of NGC 2392 is only just capable of powering the diffuse X-ray emission, a situation that can be favored by the contribution of the stellar wind from the WD companion (Miszalski et al. 2019).

## 5. SUMMARY

Inspired by the recent discovery of a spectroscopic binary companion of the CSPN of NGC 2392, we have revisited the spectral and temporal properties of its hard X-ray emission. The X-ray emission is confirmed to be one of the hardest among the X-ray emission from CSPNe, with a plasma temperature  $\simeq 26 \text{ MK}$  and an X-ray luminosity close to  $10^{31} \text{ erg s}^{-1}$ . We find evidence that the X-ray emission is modulated, with a period of 0.26 days, which is much shorter than the 1.9 days orbital period of the companion, but twice the 0.123 days rotational period of the CSPN. Coronal emission from an unseen companion falls below the levels of the observed X-ray emission, whereas the current stellar wind is not capable of producing it, either. The X-ray luminosity and temperature are consistent with those expected from the accretion of material from an unseen main-sequence companion onto the surface of the CSPN, or from accretion of the CSPN stellar wind directly onto

the surface of a WD companion. The former scenario is not supported by the different rotational period of the CSPN and time-scale of the modulation of the X-ray emission, whereas the latter scenario cannot provide an explanation for the O VI UV P-Cygni profiles present in the stellar spectrum, which still require an in-situ production of X-rays at the CSPN, maybe through shocks in the stellar wind.

The tantalizing variability of the X-ray emission from the CSPN of NGC 2392 provides another important piece of information to understand its nature and possible implications on the currently active collimation process of its fast outflows. A better assessment of this variability and its time-scale is necessary for a critical comparison with the orbital period of the WD companion and the rotational period of the CSPN. Upcoming high-sensitivity X-ray missions such as *Athena* (Nandra et al. 2013) would be able to assess and characterize the X-ray variability of the CSPN of NGC 2392 and that of other hard X-ray CSPNe because their emission can be spectrally distinguished from that of their soft diffuse emissions.

MAG acknowledges financial support by grants AYA 2014-57280-P and PGC2018-102184-B-I00, co-funded with FEDER funds, and from the State Agency for Research of the Spanish MCIU through the “Center of Excellence Severo Ochoa” award for the Instituto de Astrofísica de Andalucía (SEV-2017-0709). JAT and MAG are funded by UNAM DGAPA PAPIIT project IA100318. YHC is supported by Taiwanese Ministry of Science and Technology grant MOST 108-2811-M-001-587. We appreciate Dr. F.F. Bauer for his help to build the Lomb-Scargle periodogram and derive the false alarm probability of the light curve of the central star of the Eskimo, and an anonymous referee for useful comments. This research has made use of the SIMBAD database, operated at CDS, Strasbourg, France. Based on observations made with the Italian Telescopio Nazionale Galileo (TNG) operated on the island of La Palma by the Fundación Galileo Galilei of the INAF (Istituto Nazionale di Astrofisica) at the Spanish Observatorio del Roque de los Muchachos of the Instituto de Astrofísica de Canarias.

*Facility:* CXO (ACIS), XMM-Newton (EPIC), IUE, FUSE, ORM TNG (NICS), Spitzer (IRAC, IRS)

## REFERENCES

- Arnaud, K. A. 1996, *Astronomical Data Analysis Software and Systems V*, 101, 17
- Ayres, T. R., Linsky, J. L., Vaiana, G. S., Golub, L., & Rosner, R. 1981, *ApJ*, 250, 293

- Balucinska-Church, M., & McCammon, D. 1992, *ApJ*, 400, 699
- Barker, T. 1991, *ApJ*, 371, 217
- Berghöfer, T. W., Schmitt, J. H. M. M., Danner, R., Cassinelli, J. P. 1997, *A&A*, 322, 167
- Cardelli, J. A., Clayton, G. C., & Mathis, J. S. 1989, *ApJ*, 345, 245
- Ciardullo, R., Bond, H. E., Sipior, M. S., Fullton, L. K., Zhang, C.-Y., & Schaefer, K. G. 1999, *AJ*, 118, 488
- Danehkar, A., Frew, D. J., Parker, Q. A., et al. 2012, *IAU Symp.* 282, From Interacting Binaries to Exoplanets: Essential Modeling Tools, 470
- Eracleous, M., Halpern, J., & Patterson, J. 1991, *ApJ*, 382, 290
- Ercolano, B. 2009, *MNRAS*, 397, L69
- Eze, R. N. C., Luna, G. J. M., & Smith, R. K. 2010, *ApJ*, 709, 816
- Fazio, G. G., Hora, J. L., Allen, L. E., et al. 2004, *ApJS*, 154, 10
- Fleming, T. A., Schmitt, J. H. M. M., & Giampapa, M. S. 1995, *ApJ*, 450, 401
- Fruscione, A., McDowell, J. C., Allen, G. E., et al. 2006, *Proc. SPIE*, 62701V
- García-Díaz, M. T., Gutiérrez, L., Steffen, W., et al. 2015, *ApJ*, 798, 129
- García-Díaz, M. T., López, J. A., Steffen, W., et al. 2012, *ApJ*, 761, 172
- Giesecking, F., Becker, I., & Solf, J. 1985, *ApJL*, 295, L17
- Gondoin, P. 2000, *Stellar Clusters and Associations: Convection, Rotation, and Dynamos*, 198, 459
- Gondoin, P. 2003a, *A&A*, 409, 263
- Gondoin, P. 2003b, *A&A*, 404, 355
- Gondoin, P. 2004, *A&A*, 413, 1095
- Gondoin, P. 2005a, *A&A*, 431, 1027
- Gondoin, P. 2005b, *A&A*, 444, 531
- Gondoin, P., Erd, C., & Lumb, D. 2002, *A&A*, 383, 919
- Gregory, P. C., & Loredó, T. J. 1992, *ApJ*, 398, 146
- Güdel, M. 2004, *A&A Rv*12, 71
- Guerrero, M.A., Chu, Y.-H., Gruendl, R.A., Williams, R.M., & Kaler, J.B. 2001, *ApJ*, 553, L55
- Guerrero, M. A., Chu, Y.-H., Gruendl, R. A., & Meixner, M. 2005, *A&A*, 430, L69
- Guerrero, M. A., & De Marco, O. 2013, *A&A*, 553, A126
- Guerrero, M. A., Jaxon, E. G., & Chu, Y.-H. 2004, *AJ*, 128, 1705
- Haisch, B. M., Bookbinder, J. A., Maggio, A., Vaiana, G. S., & Bennett, J. O. 1990, *ApJ*, 361, 570
- Handler, G. 1996, *Information Bulletin on Variable Stars*, 4283, 1
- Herald, J. E., & Bianchi, L. 2011, *MNRAS*, 417, 2440
- Houck, J. R., Roellig, T. L., van Cleve, J., et al. 2004, *ApJS*, 154, 18
- Hünsch, M., Schmitt, J. H. M. M., Sterzik, M. F., & Voges, W. 1999, *A&AS*, 135, 319
- Hünsch, M., Schmitt, J. H. M. M., & Voges, W. 1998a, *A&AS*, 132, 155
- Hünsch, M., Schmitt, J. H. M. M., & Voges, W. 1998b, *A&AS*, 127, 251
- Kimeswenger, S., & Barría, D. 2018, *A&A*, 616, L2
- Maggio, A., Vaiana, G. S., Haisch, B. M., Stern, R. A., Bookbinder, J., Harnden, F. R., Jr., & Rosner, R. 1990, *ApJ*, 348, 253
- Mastrodemos, N., & Morris, M. 1998, *ApJ*, 497, 303
- Méndez, R. H., Kudritzki, R. P., & Herrero, A. 1992, *A&A*, 260, 329
- Miszalski, B., Manick, R., Van Winckel, H., et al. 2019, *PASA*, 36, e018
- Montez, R., de Marco, O., Kastner, J. H., & Chu, Y.-H. 2010, *ApJ*, 721, 1820
- Montez, R., Kastner, J. H., Balick, B., et al. 2015, *ApJ*, 800, 8
- Mürset, U., Wolff, B., & Jordan, S. 1997, *A&A*, 319, 201
- Nandra, K., Barret, D., Barcons, X., et al. 2013, *arXiv e-prints*, arXiv:1306.2307
- Nazé, Y. 2009, *A&A*, 506, 1055
- Nebot Gómez-Morán, A., & Oskinova, L. M. 2018, *A&A*, 620, A89
- O'Dell, C. R., & Ball, M. E. 1985, *ApJ*, 289, 526
- O'Dell, C. R., Balick, B., Hajian, A. R., Henney, W. J., & Burkert, A. 2002, *AJ*, 123, 3329
- O'Dell, C. R., Weiner, L. D., & Chu, Y.-H. 1990, *ApJ*, 362, 226
- Orio, M., Covington, J., & Ögelman, H. 2001, *A&A*, 373, 542
- Patriarchi, P., & Perinotto, M. 1995, *A&AS*, 110, 353
- Pauldrach, A. W. A., Hoffmann, T. L., & Méndez, R. H. 2004, *A&A*, 419, 1111
- Perryman, M. A. C., Lindegren, L., Kovalevsky, J., et al. 1997, *A&A*, 500, 501
- Pottasch, S. R., Bernard-Salas, J., & Roellig, T. L. 2008, *A&A*, 481, 393
- Prinja, R. K., & Urbaneja, M. A. 2014, *MNRAS*, 440, 2684
- Rauch T. 1997, *A&A*, 320, 237
- Reay, N. K., Atherton, P. D., & Taylor, K. 1983, *MNRAS*, 203, 1087
- Reyes-Ruiz, M., & López, J. A. 1999, *ApJ*, 524, 952
- Ruiz, N., Chu, Y.-H., Gruendl, R. A., et al. 2013, *ApJ*, 767, 35
- Sana, H., Rauw, G., Nazé, Y., Gosset, E., & Vreux, J.-M. 2006, *MNRAS*, 372, 661

Soker, N., & Kastner, J. H. 2002, ApJ, 570, 245  
Soker, N., & Livio, M. 1994, ApJ, 421, 219

Stute, M., & Sahai, R. 2009, A&A, 498, 209  
Toalá, J. A., & Arthur, S. J. 2016, MNRAS, 463, 4438